Implementation of a nonlinear filter for online nuclear counting

Romain Coulon, Jonathan Dumazert, Vladimir Kondrasovs, Stéphane Normand

Implementation of a Nonlinear Filter for Online Nuclear Counting

R. Coulon,[a,*] J. Dumazert,[a] V. Kondrasovs,[a] S. Normand[a]

[a]*CEA, LIST, Laboratoire Capteurs et Architectures Electroniques, F-91191 Gif-sur-Yvette, France.*

*Corresponding author: romain.coulon@cea.fr (+33)169088491

Elsevier use only: Received date here; revised date here; accepted date here

Highlights

- An efficient approach based on nonlinear filtering has been implemented.
- The hypothesis test provides a local maximum likelihood estimation of the count rate.
- The filter ensures an optimal compromise between precision and response time.

Abstract

Nuclear counting is a challenging task for nuclear instrumentation because of the stochastic nature of radioactivity. Event counting has to be processed and filtered to determine a stable count rate value and perform variation monitoring of the measured event. An innovative approach for nuclear counting is presented in this study, improving response time and maintaining count rate stability. Some nonlinear filters providing a local maximum likelihood estimation of the signal have been recently developed, which have been tested and compared with conventional linear filters. A nonlinear filter thus developed shows significant performance in terms of response time and measurement precision. The filter also presents the specificity of easy embedment into digital signal processor (DSP) electronics based on field-programmable gate arrays (FPGA) or microcontrollers, compatible with real-time requirements.

Keywords: Nuclear; Measurement; Filter; Signal Processing

1. Introduction

Disintegration of a radioactive source is a purely stochastic phenomenon because of the indeterministic nature and respective independence of unstable nuclei. Such a source is characterized by its half-life $T_{1/2}$ and radioactive constant $\lambda' = \ln(2)/T_{1/2}$. Nuclear measurement in pulse mode consists in estimating the output count rate λ expressed in counts per second $\lambda = \eta\lambda'$, where η is the transfer function taking into account the radiation emission probability and the intrinsic and geometric efficiencies of the sensor. This study deals with filters allowing

smoothing of the nuclear counting signal. The aim of this study is to accurately estimate the evolution of λ as a function of time t. Figure 1 illustrates the processing of a row-counting signal by two different filters. The first filter smooths the signal more efficiently than the second one, but involves a longer response time. A filter optimized according to this trade-off is thus introduced.

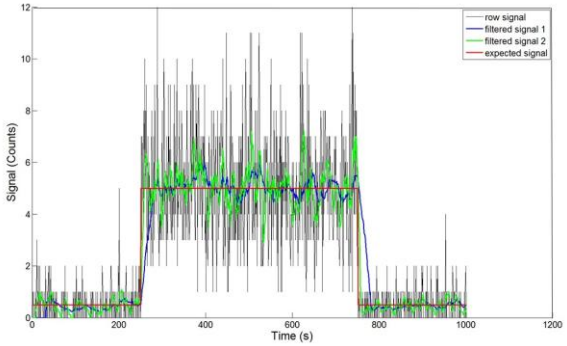

Fig. 1. Illustration of nuclear counting filtering.

As pulses are considered well separated and uncorrelated (no pile-up), the probability to count $N = n$ events during an elementary integration time interval Δt follows the Poisson law (Eq. 1), where λ is the expected count rate:[1]

$$\mathrm{P(N=n)}=\mathrm{e}^{-(\lambda\Delta \mathrm{t})}\frac{(\lambda\Delta \mathrm{t})}{\mathrm{n!}}. \quad (1)$$

Specificity of the Poisson distribution is the equality of the expected count value $\mathbb{E}[N]$ and its variance $\sigma^2(N)$:

$$\mathbb{E}[N] = \sigma^2(N) = \lambda\Delta t. \quad (2)$$

At low and constant λ, the maximum likelihood estimate $\hat{\lambda}^i_{LM}$ of the count rate over a sample of i measured count values $N_{j,1\leq j\leq i}$ is given by the empirical mean calculated during the total integration time $i\Delta t$ (Eq. 3)[2]:

$$\hat{\lambda}^i_{LM} = \frac{1}{\mathrm{i}\Delta \mathrm{t}}\sum_{j=1}^{i} N_j. \quad (3)$$

According to Eqs. 2 and 3 and considering a null variance associated with Δt, the statistical variance of $\hat{\lambda}^i_{LM}$ is evaluated as follows:

$$\sigma^2\left(\hat{\lambda}^i_{LM}\right) = \left(\frac{\partial\hat{\lambda}^i_{LM}}{\partial N_i}\right)^2 \sigma^2(N_i) = \left(\frac{1}{i\Delta t}\right)^2 \sum_{j=1}^{i} N_j. \quad (4)$$

The relative standard deviation associated with the estimation of λ with a given i is therefore expressed as

$$\frac{\sigma^2\left(\hat{\lambda}^i_{LM}\right)}{\hat{\lambda}^i_{LM}} = \frac{1}{\sqrt{\hat{\lambda}^i_{LM}\, i\Delta t}}. \quad (5)$$

The choice of the sample size i retained for the measurement therefore results in a trade-off between the response time $i\Delta t$ and the precision proportional to $1/\sqrt{i\Delta t}$, both to be minimized. As an example of Figure 1, the first and second filtered signals correspond to integration lengths $i = 8$ and 32, respectively.

The organization of this paper is as follows. First, a state of the art regarding smoothing filters applied to nuclear instrumentation is introduced. Then, implementation of the proposed CST filter is described and the method used for benchmarking the different filters is detailed. Finally, the results are presented to highlight the performance of the CST filter compared with its counterparts.

2. Related work

The main filter used in industrial implementations is labeled “Moving Average” (MA**)** and exploits the empirical mean estimator. This filter provides a different estimation for every value of i. This linear low-pass filter is suitable for estimating a nonvarying λ, but becomes nonspecific when an abrupt change in radioactivity occurs. Then, a trade-off regarding the experimental conditions and the purpose of the measurement has to be found. Indeed,

if the requirement of the system lies only within the response time performance to a variation of λ, a fixed value of i is set ("preset time ratemeter"). On the contrary, if the requirements are only to display a precise value (low fluctuation), the signal is integrated until a prefixed required statistical precision is achieved ("preset count ratemeter").[3–5] A way of reconciling both requirements may be to introduce a weighted function with factors $\mu_{j,1\leq j\leq i}$ as described in Eq. 6 (these factors are also called *forgetting factors*):

$$\hat{\lambda}_{\mu}^{i} = \frac{1}{\mathrm{i}\Delta\mathrm{t}} \frac{\sum_{j=1}^{i} N_j \mu_j}{\sum_{j=1}^{i} \mu_j}. \quad (6)$$

The most frequent implementation of this alternative to preset ratemeters is the exponential moving average (EMA), with exponential weight factors $\mu_j = exp(-\theta j)$, where θ is the parameter of the filter.[6–8] In general, finite impulse response filters have been studied earlier.[9–12] Linear filters have shown limits with regard to the trade-off between precision and response time. More recently, edge-preserving filters have been developed in nonlinear algorithms to deal with this issue.

A nonlinear strategy has been developed (SPRT and GLR filters) by several authors,[15–19] which consists in adapting the sample size i retained for a local maximum likelihood estimation according to the detection of any abrupt change in the Poisson statistics.[13,14] The detection method is based on a hypothesis testing model, and allows for making a quick decision. A nonlinear filter implementing a hypothesis test labeled CST is described in this study.

3. Implementation of the nonlinear filter

The algorithm of the CST filter is divided into schematic steps for the ease of representation. These steps are as follows: reading the new sample, calculating the estimate vector, decision made after the hypothesis test, and action performed based on the test result (Fig. 2).

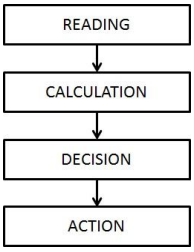

Fig. 2. Schematic view of the **CST** algorithm.

3.1. Reading and data management

For every elementary time interval Δt, event pulses are counted; at the end t of the counting interval, the count number N_1^t is recorded at the front of a memory buffer containing M slots. Before any new acquisition, all recorded values are shifted as follows:

$$\forall \mathrm{t} \in [\Delta t; T], \forall \mathrm{j} \in [2; M], \qquad N_j^t = N_{j-1}^{t-\Delta t} \quad (7)$$

3.2. Calculation of the estimation vector

A vector $\hat{\Lambda}^t$ containing count rate estimates $\hat{\lambda}_i^t$ with several retained sample sizes i associated with different response time and precision performances is found (Eq. 8). The scalar $l^t \in [1; M]$ is used to limit the size of the buffer window at time t. The primary aim of this filter is to estimate the value of i at every acquisition time t, ensuring the best compromise between response time and precision (Eq. 5):

$$\forall \mathrm{t} \in [0; T], \forall \mathrm{j} \in [1; l^t], \qquad \hat{\lambda}_i^t = \frac{1}{i} \sum_{j=1}^{i} N_j^t. \quad (8)$$

3.3. Formalism of the hypothesis test

The expected count value in counts per sample (cps) is defined as a function of the acquisition time t with λ^t. The detection test for a change in λ^t is a classical hypothesis test with null hypothesis $\mathbf{H}_0$

indicating the absence of detection and detection hypothesis $\mathbf{H}_1$ indicating the presence of detection (Eq. 9), where γ_0 is the initial count rate level, γ_1 is a new signal level after variation, and w^t is the value of i at which the change occurs:

$$\mathbf{H}_0: \quad \forall i \in [0; l^t], \quad \lambda^{t-i\Delta t} = \gamma_0 \qquad (9)$$

$$\mathbf{H}_1: \quad \exists w^t \in [0; l^t] / \quad \lambda^{t-i\Delta t} = \gamma_0 \text{ for } 1 \leq i \leq w^t \qquad (10)$$

$$\lambda^{t-i\Delta t} = \gamma_1 \text{ for } w^t \leq i \leq l^t \qquad (11)$$

3.4. Decision tests

The first solution was proposed by Coop and Fehlau.[15,16] They implemented a sequential probability ratio test (SPRT), where the background level γ_0 is determined from previous estimates and the expected jump level γ_1 is a preset parameter. In order to avoid presetting values for γ_1, Apostolopoulos developed a window-limited generalized likelihood ratio (GLR) test[17–19] based on the double maximization of a test function according to both unknowns γ_1 and w^t. An alternative hypothesis test named CST (Centered Significance Test) is proposed by the authors of this study.[20]

The detection is based on a significance test on count rate difference. In order to determine the position of a significant change w^t at time t, based on the previously selected integration window l^t, every estimate $\hat{\lambda}_i^t$ is compared with the estimate $\hat{\lambda}_{l^t}^t$. A variation vector $\Delta\hat{\lambda}^t$ is expressed as follows:

$$\forall i \in [1; l^t], \qquad \Delta\hat{\lambda}_i^t = \hat{\lambda}_{l^t}^t - \hat{\lambda}_i^t \,. \quad (12)$$

If $\mathbf{H}_0$ is verified as the difference of two count rate estimators under the same λ, the value of $\Delta\hat{\lambda}_{l^t}^t$ could be considered as null. The variance $\sigma^2(\Delta\hat{\lambda}_i^t)$ is estimated as the sum of both count rate variances $\sigma^2(\hat{\lambda}_{l^t}^t)$ and $\sigma^2(\hat{\lambda}_i^t)$ (according to the Poisson distribution) as described in Eqs. 13 and 14:

$$\sigma^2(\Delta\hat{\lambda}_i^t) = \sigma^2(\hat{\lambda}_{l^t}^t) + \sigma^2(\hat{\lambda}_i^t) \quad (13)$$

$$\sigma^2(\Delta\hat{\lambda}_i^t) = \frac{\hat{\lambda}_{l^t}^t}{l^t} + \frac{\hat{\lambda}_i^t}{i} \,. \quad (14)$$

As a result, any change in λ^t leads to the rejection of the null hypothesis. We introduce $\alpha = p(\mathbf{H}_1/\mathbf{H}_0)$ as the probability of false detection. The distribution associates a quantile t_α to the value of α governing the risk of not detecting a change in λ under $\mathbf{H}_1$. Figure 3 shows the relationship between the probability α and the coverage factor t_α used in the test. Values of α are derived from a numerical calculation using randomly generated count values over a Poisson distribution. The data are scanned from the slot $i = 1$ to the slot $i = l^t$ to process the detection tests presented in Eqs.15 and 16:

$$If: \quad \forall i \in [1; l^t], \left|\Delta\hat{\lambda}_i^t\right| \leq t_\alpha \sigma(\Delta\hat{\lambda}_i^t), \quad (15)$$

then the hypothesis $\mathbf{H}_0$ is accepted and $\mathbf{H}_1$ is rejected;

$$If: \quad \exists i \in [1; l^t], \left|\Delta\hat{\lambda}_i^t\right| > t_\alpha \sigma(\Delta\hat{\lambda}_i^t), \quad (16)$$

then the hypothesis $\mathbf{H}_0$ is rejected and $\mathbf{H}_1$ is accepted.

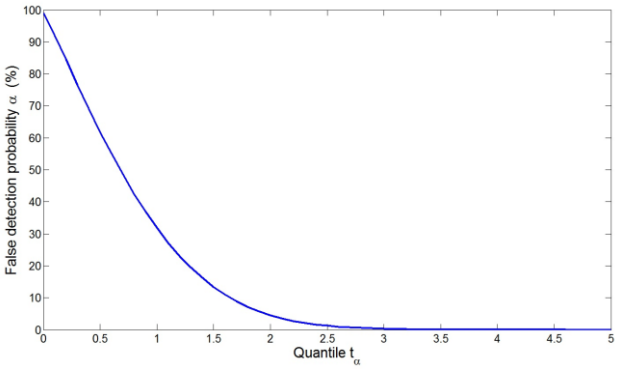

Fig. 3. Relationship between confidence level α and coverage factor t_α.

3.5. Action following the test

Regarding the result of the test, one of the following actions is performed:

- If $\mathbf{H}_0$ is accepted for all the slots $1 \leq i \leq l^t$, the number of allocated buffer slots is extended: $l^{t+\Delta t} = l^t + 1$.

- If $\mathbf{H}_1$ is accepted for a slot number w^t, a change in signal is considered significant. The number of allocated slots is reduced by φ slots, where φ equals the number of slots verifying the condition of rejection specified in Eq. 16:

$$l^{t+\Delta t} = l^t - \varphi. \quad (16)$$

The value $\hat{\lambda}^t_{l^{t+\Delta t}}$ is finally transmitted at the output of the filter as the current count rate.

4. Test bench for the filters

A test bench was built to assess the performance of the following online filters:

- The moving average (MA) most commonly implemented into preset time ratemeters[3] (Eq. 3).
- The exponential moving average (EMA)[6–8] (Eq. 6), where θ is the degree of freedom in the design.
- The nonlinear filter introduced in ref. [19] and labeled GLR**,** where the threshold h is the degree of freedom in the design.
- The nonlinear filter proposed in this study, previously introduced in ref. [20] and labeled CST, where the quantile t_α is the degree of freedom in the design.

The counting signal is simulated using a Poisson distribution generated as a function of count expectation as presented in ref. [21]. All filters need to be assessed for precision, accuracy, and response time performance as defined in the international standard IEC 60325 related to radiation monitoring.[22] Filters are tested under two sets of simulated signals. The first is a static signal with a constant count expectation γ_0, allowing the evaluation of precision and accuracy of the filter. The second is a dynamic signal where the expected count value is changed by one decade, allowing the estimation of response time of the filter.

4.1. Static performance

A counting signal with a constant count expectation is generated over z samples: $\forall j \in [1; z], \lambda_j = \gamma_0$. The empirical mean $\bar{\lambda}$ and standard deviation $\sigma(\lambda)$ over the different filter results $\hat{\lambda}_j$ obtained with the algorithms previously detailed are calculated by Eqs. 17 and 18, respectively, as follows:

$$\bar{\lambda} = \frac{1}{z}\sum_{j=1}^{z} \hat{\lambda}_j \quad (17)$$

$$\sigma(\lambda) = \sqrt{\frac{1}{z}\sum_{j=1}^{z}\left(\hat{\lambda}_j - \bar{\lambda}\right)^2}. \quad (18)$$

The mean provides by construction an unbiased estimate of the Poisson count rate. Both nonlinear filters GLR and CST are based on a moving average over an adaptable number of samples (l^t for the CST): these filters are therefore unbiased as long as their activity remains constant.

The factor of merit $\mathcal{P}$ allows us to evaluate the level of precision achieved with a given filter. The filtering is repeated x times and the results are stored in frames labeled $f = 1 \ldots x$. $\mathcal{P}_f$ is defined as the average ratio of the empirical standard deviation $\sigma(\lambda_f)$ for every f between 1 and x to the empirical mean $\bar{\lambda}_f$ for every f between 1 and x:

$$\mathcal{P} = \frac{1}{x}\sum_{f=1}^{x} \mathcal{P}_f = \frac{1}{x}\sum_{f=1}^{x} \frac{\sigma(\lambda_f)}{\bar{\lambda}_f} \quad (19)$$

$$\sigma(\mathcal{P}) = \sqrt{\frac{1}{x}\sum_{f=1}^{x}\left(\mathcal{P}_f - \mathcal{P}\right)^2}. \quad (20)$$

4.2. Dynamic performance

The response of the filter to an increase of one decade of the expected count rate $\gamma_1 = 10\gamma_0$ is studied according to international standard.[22] Counts are generated in the following pattern:

$$\forall j \in [1;250], \quad \lambda_j = \gamma_0 \quad (21)$$
$$\forall j \in [250;750], \quad \lambda_j = \gamma_1 \quad (22)$$
$$\forall j \in [750;1000], \quad \lambda_j = \gamma_0. \quad (23)$$

Count values are generated following this pattern over x iterations. The increase time $\tau_{inc,f}$ (defined as the time necessary to account for a γ_0 to γ_1 evolution) and decrease time of the frame f, $\tau_{dec,f}$ (defined as the time necessary to account for a γ_1 to γ_0 evolution) are calculated for every frame $f \in [1;x]$ (Eqs. 24 and 26):

$$\tau_{inc,f} = \underset{j\in[250;270]}{\operatorname{argmin}} \left\{\hat{\lambda}_j > 0.9\gamma_1\right\} \quad (24)$$

$$\tau_{inc,f} = \underset{j\in[500;1000]}{\operatorname{argmin}} \left\{\hat{\lambda}_j > 1.1\gamma_0\right\}. \quad (25)$$

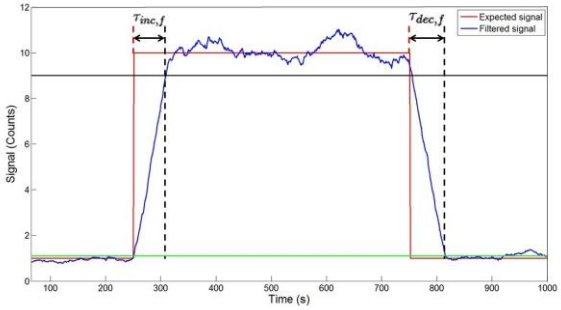

Fig. 4. Calculation of $\tau_{inc,f}$ and $\tau_{dec,f}$.

We introduce for every tabulated value of the response times τ_{inc} and τ_{dec} the number of occurrences $\omega_{\tau_{inc}}$ and $\omega_{\tau_{dec}}$. For both response times, we retain the values of $\hat{\tau}_{inc}$ and $\hat{\tau}_{dec}$ so that 80% of the distribution falls below these thresholds (Fig. 5):

$$\hat{\tau}_{inc} = \underset{\tau_{inc}}{\operatorname{argmin}} \left\{\int_0^{\tau_{inc}} \omega_{\tau_{inc}} d\tau_{inc} > 0.8\right\} \quad (26)$$

$$\hat{\tau}_{dec} = \underset{\tau_{dec}}{\operatorname{argmin}} \left\{\int_0^{\tau_{dec}} \omega_{\tau_{dec}} d\tau_{dec} > 0.8\right\} \quad (27)$$

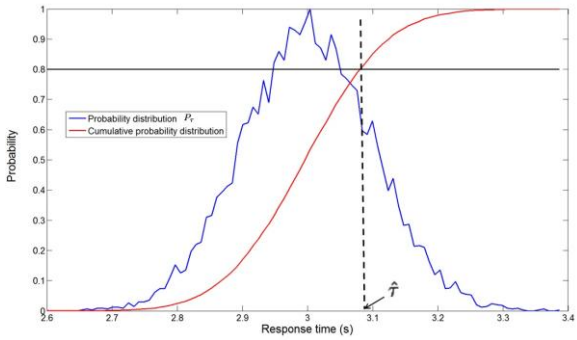

Fig. 5. Calculation of $\hat{\tau}$.

4.3. Figure of merit

An indicator has to be built to quantify the trade-off between precision and response time. A figure of merit labeled FOM is computed for any given filter X by multiplying the precision obtained in static conditions $\mathcal{P}$ and the summation of the increase time τ_{inc} and decrease time τ_{dec}. The obtained product is normalized by the MA filter product as follows:

$$FOM(X) = \frac{\mathcal{P}(X)[\tau_{inc}(X) + \tau_{dec}(X)]}{\mathcal{P}(MA)[\tau_{inc}(MA) + \tau_{dec}(MA)]}. \quad (28)$$

Considering that individual terms are uncorrelated, the cumulative variance $\sigma^2(FOM(X))$ associated with the FOM is determined as:

$$\sigma^2(FOM(X)) =$$

$$\left[\frac{\mathcal{P}(X)}{\mathcal{P}(MA)[\tau_{inc}(MA) + \tau_{dec}(MA)]}\right]^2 \left[\sigma^2(\tau_{inc}(X)) + \sigma^2(\tau_{dec}(X))\right]$$

$$+\left[\frac{\tau_{inc}(X) + \tau_{dec}(X)}{\mathcal{P}(MA)[\tau_{inc}(MA) + \tau_{dec}(MA)]}\right]^2 \sigma^2(\mathcal{P}(X))$$

$$+\left[\frac{\mathcal{P}(X)[\tau_{inc}(X)+\tau_{dec}(X)]}{\mathcal{P}(MA)^2[\tau_{inc}(MA)+\tau_{dec}(MA)]}\right]^2\sigma^2\big(\mathcal{P}(MA)\big)$$

$$+\left[\frac{\mathcal{P}(X)[\tau_{inc}(X)+\tau_{dec}(X)]}{\mathcal{P}(MA)[\tau_{inc}(MA)+\tau_{dec}(MA)]^2}\right]^2$$

$$\times\left[\sigma^2\big(\tau_{inc}(X)\big)+\sigma^2\big(\tau_{dec}(X)\big)\right]. \quad (29)$$

$FOM = 1$ indicates that the filter provides no significant gain in comparison to the reference MA filter; $FOM > 1$ indicates non specificity of the filter; and $FOM < 1$ quantifies the improvement ensured by the filter in comparison to the MA filter concerning the compromise between response time and precision.

5. Results

5.1. Influence of parameters

Every filter was tested for different values of the parameters, and compared to the MA filter using a number of recorded count rate values of $M = 64$. The parameters θ_k, h_k, and $t_{\alpha,k}$ are defined by the index k as follows:

$\forall k \in [1;20]$,

$$\theta_k = 0.05k \quad (30)$$
$$h_k = 0.5k \quad (31)$$
$$t_{\alpha,k} = 0.2k \quad (32)$$

Figure 6 shows the evolution of precision $\mathcal{P}$ as a function of parameters used in each filter for an activity of 100 cps. We can observe that the precision of the EMA filter decreases continuously with the increase of θ. On the contrary, CST and GLR filters exhibit a drastic improvement of precision with the increase of t_α and h reaching the asymptotic minimal standard deviation when the index k reaches a value >8 and >10, respectively, which corresponds to $t_\alpha = 2$ and $h = 5$. A stable curve is observed when a change in count rate occurs.

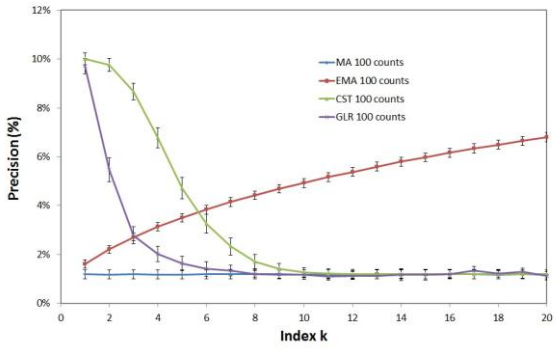

Fig. 6. Relative standard deviation as a function of parameters at a count rate of 100 cps (M = 64).

The evolution of increase time as a function of the parameters is presented in Figure 7. The response time to an increase step of activity is monotonously decreased by the increase of θ for the EMA filter and monotonously increased by the increase of t_α and h for the CST and GLR filters. If t_α or h is chosen below the index value $k = 8$, a significant improvement of the response time is observed by the use of nonlinear filters compared with the linear ones. A similar improvement is noted for decrease time (Fig. 8). A stable curve is observed when a change in count rate occurs.

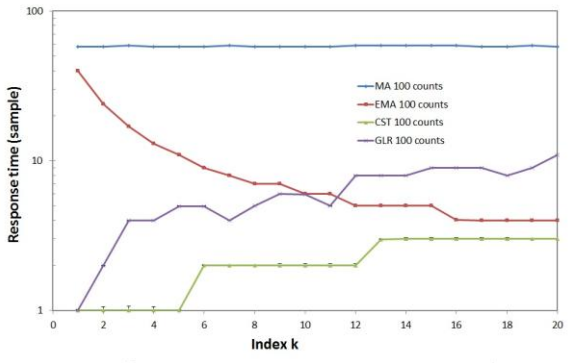

Fig. 7. Increase time as a function of parameters for an increase step of activity such as $\gamma_1 = 100$ cps and $\gamma_1 = 1000$ cps ($M = 64$).

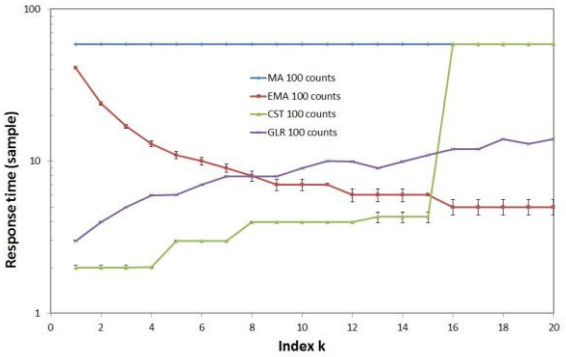

Fig. 8. Decrease time as a function of parameters for an increase step of activity such as $\gamma_1 = 100$ cps and $\gamma_1 = 10$ cps ($M = 64$).

Optimal values for the parameters eventually have to be determined according to the best compromise between precision and response time, which corresponds to the "elbow" of the characteristics displayed in Figure 9. The values of the relative standard deviation $\mathcal{P}_{\gamma_0}$ are displayed as a function of response time τ_{γ_0}, where $\mathcal{P}$ and τ are averaged over different expected count values ($\gamma_0 = \{0.1, 1, 10, 100\}$ cps). An average behavior of the filters is thus obtained. It can be immediately observed that the coordinates of the elbows on the CST curves fall below the coordinates of the elbows on the GLR and EMA curves. Therefore, in order to provide the best compromise between precision and response time, the following parameters are retained for each filter:

- EMA filter: $\theta = 0.7 \pm 0.1$,
- GLR filter: $h = 1.5 \pm 0.5$,
- EMA filter: $t_\alpha = 1.6 \pm 0.2$ ($\alpha = 10\%$).

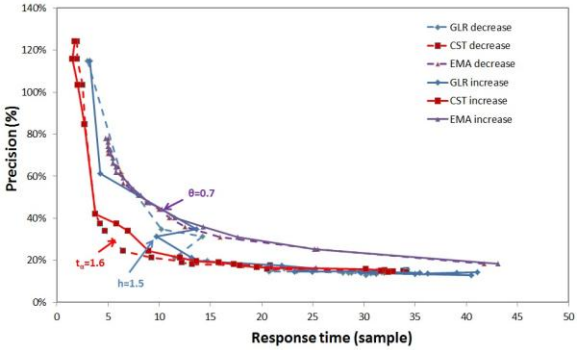

Fig. 9. Relative standard deviation $\mathcal{P}_{\gamma_0}$ as a function of response time τ_{γ_0} for different parameter values ($M = 64$).

These values of the parameters are used in the rest of this dissertation.

5.2. Influence of count rate expectation

The evolution of the precision $\mathcal{P}$ as a function of the expected count rate γ_0 varying between 0.1 and 1000 counts per sample is presented in Figure 10. As theoretically known from Eq. 5, the precision follows a law in the inverse of the square root of the expected count rate. For a given count rate intensity and using the parameters previously determined, the best precision is achieved by the MA estimation, followed by the GLR, CST and EMA. The precisions of the different filters are compared with the reference precision obtained with the MA filter. The results are presented as follows:

- $\mathcal{P}_{GLR} = 1.2\,\mathcal{P}_{MA}$,
- $\mathcal{P}_{CST} = 1.7\,\mathcal{P}_{MA}$,
- $\mathcal{P}_{EMA} = 4.9\,\mathcal{P}_{MA}$.

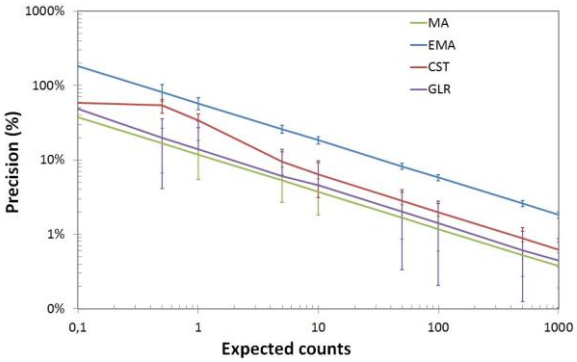

Fig. 10. Relative standard deviation P as a function of the expected count rate γ_0 ($M = 64$).

The evolution of response time t_{inc} to an increase step of activity (such as $\gamma_1 = 10\,\gamma_0$) as a function of the initial count rate value γ_0 from 0.01 to 1000 counts per sample is presented in Figure 11. The MA filter provides the longest response time: between 95 and 60 samples below a count rate γ_0 = 1 cps and 60 samples above it. The EMA filter exhibits a

response time compromised between 20 and five samples over the entire range of count rates. The EMA filter is dramatically faster than the MA filter (12 times faster with a five times poorer precision). At low count rate (<1 cps), the GRL does not show any significant improvement in terms of response time and the CST does not achieve the responsivity of the EMA, although it still provides a noticeable gain compared with the MA filter (two to three times faster). At medium and higher count rates (>1 cps), the nonlinear filters GLR and CST present an important gain in response time when compared with linear filters. Indeed, the CST and GLR response times represent only two samples, whereas the EMA requires five samples and the MA filter about 60 samples. A similar behavior is observed for the response to a decrease step of activity (Fig. 12).

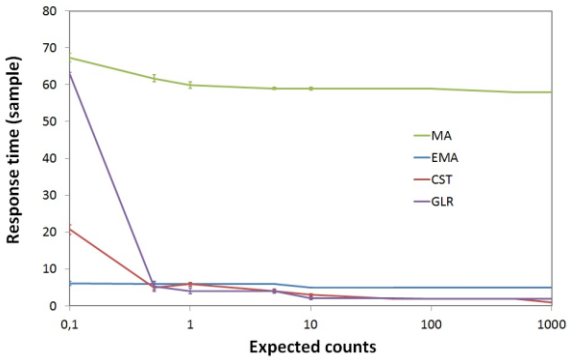

Fig. 11. Response time τ_{inc} as a function of the initial count rate γ_0 ($M = 64$).

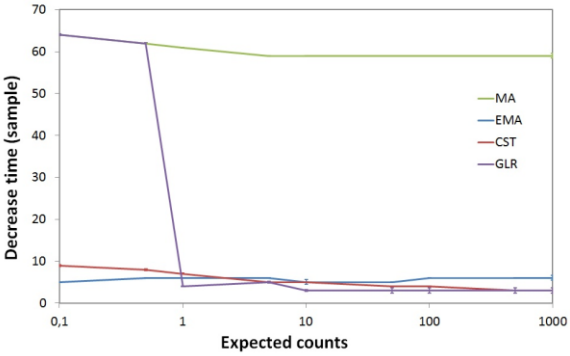

Fig. 12. Response time τ_{dec} as a function of the initial count rate γ_0 ($M = 64$).

In order to consider both precision and response time, the FOM are presented in Figure 13 and the key features are reported in Table 1. At low count rates (<1 cps), where the lack of information to describe the signal is critical (several null counts), all filters encounter difficulties. Under this range of count rates, the GLR filter presents a poorer FOM than the MA filter. Moreover, EMA and CST filters show only a slight gain compared with the time destructive MA filter. At medium and high count rates (>1 cps), a significant gain is showed by the nonlinear filters GLR and CST ($FOM_{GLR} = 0.6$, $FOM_{GLR} = 0.9$) compared with the linear MA and EMA filters. Therefore, advantages of nonlinear filters for ratemeter applications are clearly demonstrated. We can also conclude that the CST filter appears to present the highest performance combining a satisfactory compromise between response time and precision over the whole range of studied count rate values. This filter thus overcomes the problems associated with nuclear counting over a large and abrupt dynamic of count rates.

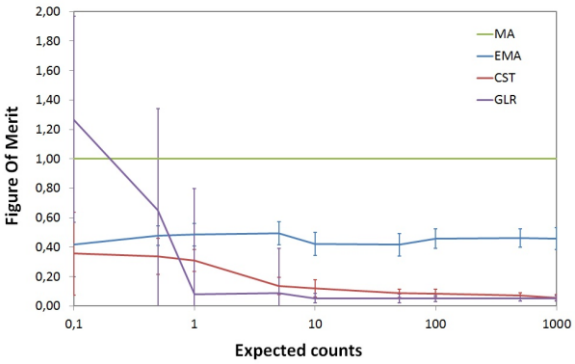

Fig. 13. Figures of merit FOM obtained as a function of count level ($M = 64$).

Table 1. Key features of the test bench.

Count rate range	Filter	Prec. $\mathcal{P}$ (%)	Inc. time τ_{inc} (sample)	Dec. time τ_{dec} (sample)	Fig. of merit FOM
Low count rate [0.1; 1] cps	**MA**	48.5	71.7	63.1	1.00
	EMA	238	8.2	51.8	0.48
	GLR	97.9	45.0	23.2	1.24
	CST	69.4	23.2	51.7	0.47
Med./High count rate]1; 1000] cps	**MA**	2.1	58.7	59.0	1.00
	EMA	10.4	5.2	5.67	0.45
	GLR	2.5	2.3	3.33	0.06
	CST	3.7	2.3	4.00	0.09

5.3. Influence of buffer size

The size of the memory buffer governs the value of the best achievable precision. It is therefore necessary to implement the algorithm with the largest size of buffer available at the hardware level. Figure 14 shows the evolution of FOM as a function of buffer size M for an activity of 50 cps. It is interesting to note that the improvement ensured by the nonlinear filters is already significant for a small buffer size ($M = 8$ samples).

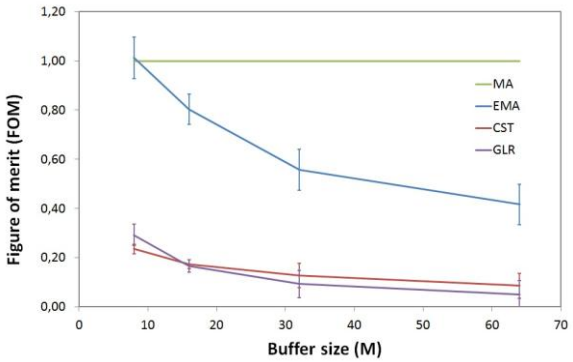

Fig. 14. Figures of merit FOM obtained at 50 counts as a function of buffer size M.

5.4. Conclusion

When compared to conventional linear filters, nonlinear filters based on a hypothesis test method exhibit significantly improved figures of merit: an important gain in response time compared with linear filters is observed, together with a reasonable degradation of precision. For applications in the fields of homeland security and health physics, guaranteeing a high sensitivity in a short timescale is critical. Thus, the fast response ensured by a nonlinear filter algorithm makes any detector based on this technique compatible with implementations requiring human responsiveness.

The simplicity of this implementation makes the CST algorithm relevant for a broad range of industrial applications, including process monitoring, area monitoring, health physics monitoring, and embedded detection.[23,24] The CST filter was implemented into a Geiger–Müller probe and set on a robot designed to address safeguard and security issues, and it is proved effective for tracking and detecting a radioactive source during a terrorist attack simulation.[25–27]

Acknowledgments

The authors would like to thank Thierry Montagu and Mathieu Thevenin for their help in the preparation of this manuscript.

References

[1] G.F. Knoll, *Radiation detection and measurement*, edited by Wiley, NY, Vol. 4 (1989), p. 65-105.

[2] G. Rodriguez, *Generalized Linear Models*, edited by Princeton University, Vol. 4 (2007), p. 1-14.

[3] C.H. Vincent, *Nuc. Ins. Meth.*, 23 (1963) 193.

[4] I.D. Vankov, G.S. Ganev, M. Ivanov and M. Müller, *Nuc. Ins. Meth*., 214 (1983) 395.

[5] V. Arandjelovic, A. Koturovic and R. Vukanovic, *Nuc. Ins. Meth*., 481(2002) 769.

[6] P. Dumesnil and J.L. Greco, *Proc. ESARDA Symp. Safe. Nuc. Mat. Man.*, (1985).

[7] Savic Z., *Nuc. Ins. Meth.*, 301 (1991) 517.

[8] H.-J Jeong, et al., *Rad. Prot. Dos.*, (2008) 1.
[9] S.J. Rudnick, P.L. Michaud and K.G. Porges K.G., *Nuc. Ins. Meth*., 71 (1969) 196.
[10] J.S. Byrd, *Nuc. Ins. Meth.*, 121 (1974) 397.
[11] G. White, *Nuc. Ins. Meth*., 125 (1975) 313.
[12] R.M. Longden-Thurgood and J. Pople, *Nuc. Ins. Meth*., 184 (1981) 533.
[13] A. Charnes, E.L. Frome and P.L. Yu, *J. Am. Stat. Ass*., 71 (1976) 214.
[14] M. Basseville M. and I.V. Nikiforov, *Detection of Abrupt Changes: Theory and Application*, edited by Prentice-Hall 1993.
[15] K. Coop, *IEEE Trans. Nuc. Sci*., 32 (1985) 934.
[16] P. Fehlau, *IEEE Trans. Nuc. Sci*., 40 (1993) 143.
[17] A. Willsky and H. Jones, *IEEE Trans. Autom. Cont*., 21 (1976) 108.
[18] A. Collura, et al., *The Astro. Journ*., 315 (1987) 340.
[19] G. Apostolopoulos, *Nuc. Ins. Meth. A*, 595 (2008) 464.
[20] V. Kondrasovs, and R. Coulon, and S. Normand, *Proc. of ANIMMA*, (2013).
[21] L. Devroye, *Non-uniform random variate generation*, Springer 1986.
[22] IEC 60325 Standard, *Radiation protection instrumentation. Apha, beta and alpha/beta contamination meters and monitors*, 2002.
[23] R. Coulon et al., *Nuc. Eng. Des*., 241 (2011) 339.
[24] K. Boudergui et al., *Proc. of ANIMMA*, (2011) .
[25] V. Kondrasovs, R. Coulon and S. Normand, Patent WO 2011101323 A1, (2011).
[26] R. Coulon, et. al., *IEEE Trans. Nuc. Sci*., 61 (2014) 2189.
[27] S. Bouchet, et al., *Proc. of WISG* (2010).